

A FREQUENCY GLITCH IN AN ACCRETING PULSAR

D. K. GALLOWAY, E. H. MORGAN, A. M. LEVINE

Center for Space Research, MIT, 37-626b, 77 Massachusetts Avenue, Cambridge, MA 02139-4307

Accepted by *ApJ*

ABSTRACT

Frequency glitches have been observed so far only in radio pulsars and anomalous X-ray pulsars. Here we present evidence of a glitch in a neutron star accreting from a Be companion. The transient KS 1947+300 reappeared in 2000 October as a moderately strong X-ray source that exhibited 18.7 s pulsations, leading to an identification with the BATSE source GRO J1948+32, last detected in 1994. We have analyzed Rossi X-ray Timing Explorer observations taken during the 2000–01 outburst, as well as additional observations taken during a smaller outburst in July 2002. Orbital Doppler shifts are apparent in the temporal variation of the pulse frequency. A joint fit of the *RXTE* data together with BATSE measurements from an outburst in 1994 yields the orbital period $P_{orb} = 40.415 \pm 0.010$ d, the projected orbital radius $a_x \sin i = 137 \pm 3$ lt-s, and the eccentricity $e = 0.033 \pm 0.013$. This degree of eccentricity is unexpectedly low for such a wide orbit. Pulse timing results also show that the intrinsic pulse frequency increased from 53.30 to 53.47 mHz at a rate approximately proportional to the X-ray flux. This is about the degree of spin up expected from the accretion torques that must be present when the X-ray luminosity reaches $\sim 10^{38}$ ergs s⁻¹. On one occasion during the 2000–01 outburst, the pulse frequency increased by $\sim 1.8 \times 10^{-6}$ Hz in $\lesssim 10$ hr over and above the mean trend seen around that time, without any indication of a correspondingly large increase in X-ray flux. The fractional change in frequency of 3.7×10^{-5} during this event is significantly larger than the values observed in the glitches in radio pulsars and anomalous X-ray pulsars. We discuss other similarities and differences between these events.

Subject headings: accretion — pulsars: general — pulsars: individual (KS 1947+300) — X-rays: stars

1. INTRODUCTION

Abrupt changes (“glitches”) in the spin frequency of rotating neutron stars have been observed to date in radio pulsars (e.g. Krawczyk et al. 2003) and anomalous X-ray pulsars (AXPs; e.g. Kaspi et al. 2003; Kaspi & Gavriil 2003). These events appear as sudden increases in the observed pulse frequency, superimposed on more-or-less steady spin-down arising from magneto-dipole braking, and are attributed to a sudden transfer of angular momentum between the superfluid of the interior and the crust (Ruderman 1976; Anderson & Itoh 1975). Between glitches the interior superfluid and the crust are relatively loosely coupled, and the braking torque acts primarily on the crust, so that just prior to a glitch the crust is spinning slower than the interior superfluid.

To date there have been no reports of glitches in accreting pulsars. Here we present the results of a pulse timing analysis of data obtained from *Rossi X-ray Timing Explorer* (*RXTE*) observations of the accreting pulsar KS 1947+300, from which we derive orbital parameters as well as the intrinsic spin frequency history of the neutron star. The latter includes a short time interval during which the pulse frequency increased at an unusually high rate, that may be the first evidence for a frequency glitch similar to those observed in radio pulsars and AXPs.

The cosmic X-ray source KS 1947+300 ($l^{II} = 66^\circ 09'$, $b^{II} = +2^\circ 10'$) was first detected on 1989 June 8 with the TTM coded mask imaging spectrometer mounted on *Mir*'s Kvant module (Skinner 1989; Borozdin et al. 1990). The optical counterpart is a $V = 14.2$ B0Ve star with moderate reddening that indicates the distance to

the system is ≈ 10 kpc (Negueruela et al. 2003). In 1994 the Burst and Transient Source Experiment (BATSE) aboard the *Compton Gamma Ray Observatory* (*CGRO*) detected 18.7 s pulsations from an X-ray source within a few degrees of KS 1947+300. From the BATSE data, Chakrabarty et al. (1995) found that the apparent pulse period of GRO J1948+32, as the pulsating source was designated, varied systematically over the 33 d outburst, indicating that the source was in a binary system with an orbital period between 35 and 44 days. In 2000 November, weak emission from KS 1947+300 was detected with the All-Sky Monitor (ASM) aboard *RXTE*. A search for periodicities in the ~ 5 yr ensemble of ASM measurements of KS 1947+300 accumulated up until that time yielded evidence of a 41.7 ± 0.1 day periodicity (Levine & Corbet 2000). Soon afterwards, pulsations with a period of 18.7 s were found in follow-up observations with the Proportional Counter Array (PCA) on *RXTE*, which showed that KS 1947+300 and GRO J1948+32 are one and the same (Swank & Morgan 2000). A series of *RXTE* target-of-opportunity (TOO) observations were then conducted which, together with the measurements by the ASM, gave excellent coverage over a long and strong outburst.

2. OBSERVATIONS AND ANALYSIS

We made observations of KS 1947+300 with all three instruments aboard *RXTE*: the ASM, PCA and the High-Energy X-ray Timing Experiment (HEXTE). The ASM views much of the sky every few hours (Levine et al. 1996). The instrument consists of three Scanning Shadow Cameras (SSCs) mounted on a rotating platform, and carries out sequences of 90 s observations

arXiv:astro-ph/0401476v2 11 Jun 2004

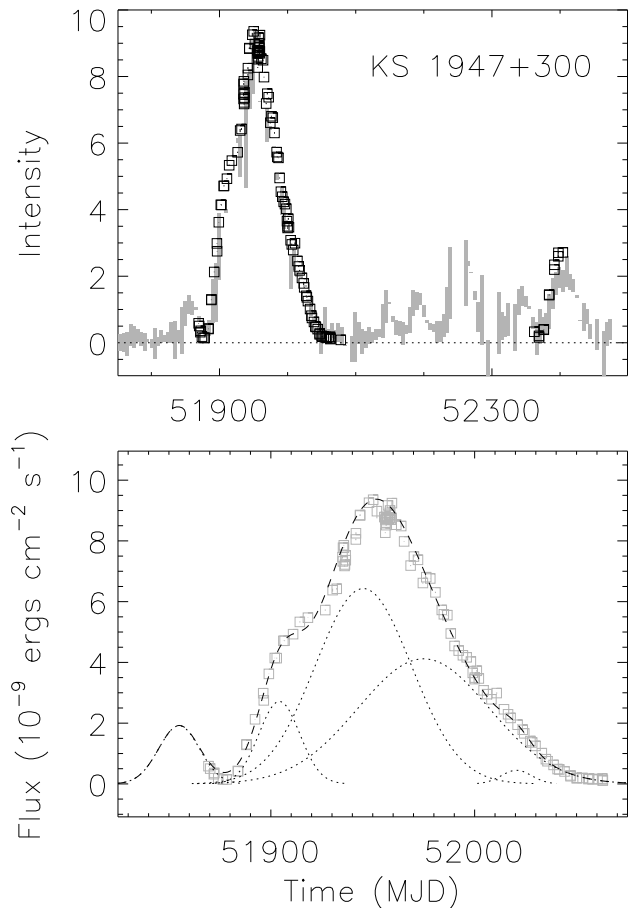


FIG. 1.— Intensity of KS 1947+300 throughout the 2000–01 outburst. (*upper panel*) The gray markers show the ASM count rate (1.5–12 keV) 1σ confidence regions (with scale on the left in ASM counts s^{-1}), from 1 day averages of 90 s dwells, smoothed over a 5-d window (excluding those with estimated 1σ errors greater than 0.7 counts s^{-1}). The open squares show the integrated 2–60 keV source flux (with scale on the left in units of 10^{-9} ergs cm^{-2} s^{-1}) as measured from best-fit models of PCA and HEXTE spectra. MJD 52000 corresponds to 2001 April 1. (*lower panel*) The flux measurements are plotted as squares on an expanded time axis, along with the individual Gaussian components (dotted lines) used to model the flux evolution, and the total model (dashed line; see §4.2).

called dwells, in between which the platform holding the SSCs is rotated by 6° . The data from each SSC are analyzed to obtain estimates of the intensities of all the sources listed in the ASM analysis catalog within the field of view. The intensities are expressed as the count rate expected from a source at the center of the field of view of SSC 1 in 1996 March¹

The ASM 1.5–12 keV intensity measurements of KS 1947+300 from 2000 July through 2002 April are shown in Fig. 1. The source became active in 2000 October and rose to an intensity of approximately 1 count s^{-1} around 2000 November 7 (MJD 51855). Following this initial peak the intensity declined somewhat before beginning a second, more substantial increase which peaked around MJD 51950 at ~ 9 counts s^{-1} (approximately

¹ The Crab Nebula appears in the ASM as a 75 count s^{-1} source (1.5–12 keV) and has a corresponding energy flux in that energy band of $\sim 2.7 \times 10^{-8}$ ergs cm^{-2} s^{-1} .

120 mCrab). Following the outburst maximum, the source declined to < 1 count s^{-1} , but subsequently exhibited a number of small outbursts peaking at 1–3 count s^{-1} and lasting for 10–50 d. The source was not detected by the ASM prior to MJD 51800; the intensity was $\lesssim 0.2$ counts s^{-1} . Relatively few measurements were taken around MJD 51960, and again around MJD 52290, when the Sun was relatively near its closest angular distance of $\sim 50^\circ$ from the source. In addition, the measurements taken close to those times were more strongly affected by systematic problems than measurements at other times.

In 2000 November, shortly after the outburst was noticed in the ASM data, a series of observations with the PCA and HEXTE aboard *RXTE* was initiated. The PCA consists of 5 Proportional Counter Units (PCUs) sensitive to X-ray photons in the range 2.5–90 keV, each with a collecting area of ~ 1400 cm^2 and a 1° field of view (Jahoda et al. 1996). Photon arrival times are measured to ≈ 1 μs . Spectra are accumulated in up to 256 energy channels. The number of PCUs operating during the observations varied between 2 and 5. The HEXTE comprises two clusters, each of which contains 4 scintillation detectors sensitive to photons in the range 15–250 keV, collimated to view a common 1° field (Gruber et al. 1996). The detectors in the two clusters provide a total collecting area of 1600 cm^2 .

The first PCA/HEXTE observation of KS 1947+300 was performed on 2000 November 21 (MJD 51869). Subsequently, 1–6 ks long PCA/HEXTE observations were made every 1–2 days until the end of the main outburst around 2001 June 18 (MJD 52078). Near the peak of the main outburst two long observations were made (for proposal ID 50068, PI: W. Heindl) that yielded 51 and 98 ks of exposure, respectively. In order to obtain a longer baseline for determination of the orbital period, an additional series of observations began on 2002 March 29 (MJD 52362) and continued until 2002 May 17 (MJD 52411). In all, 132 observations were made with a total observing time of 371 ks.

Spectral analysis of the PCA and HEXTE data was undertaken using LHEASOFT release 5.1 (2001 June 26). The data were first screened to ensure that the center of the fields of view were within 0.02° of the direction of KS 1947+300 and that the limb of the Earth was more than 10° from the source direction. Mean energy, i.e., pulse height, spectra were extracted for each observation from standard observing modes (“Standard-2”, with 129 channels between 2–60 keV for PCA, and “Archive”, with 64 channels between 15–250 keV for HEXTE). PCA spectra were accumulated separately for each PCU. Instrument response matrices were generated for each PCU and each observation using PCARSP. We estimated background count rates in the PCA using either faint or bright source models (depending upon whether the count rate exceeded ≈ 40 counts s^{-1} PCU $^{-1}$) developed for gain epoch 5 (from 2000 May 13 onwards) with PCABACKEST version 2.1e. We measured fluxes by integrating model fits to PCA and HEXTE spectra (see §3).

Pulse timing analyses were performed using software written by the *RXTE* team at MIT. For timing analysis, the 3–12 keV energy range was found to provide nearly optimal signal-to-noise ratios during the faintest observations in which we could detect pulsations. Thus

we selected, from “GoodXenon” mode data, only those events within the energy range 3–12 keV detected in the top layer of any PCU, adjusted the times of the events according to the projected distance of the spacecraft from the Solar System barycenter, and binned the selected events into 0.25 s time bins.

3. SPECTRUM

We fitted various continuum models to PCA spectra in the range 2–25 keV and HEXTE spectra in the range 15–80 keV using XSPEC version 11.0. Above a flux of $\approx 8 \times 10^{-10}$ ergs cm $^{-2}$ s $^{-1}$ (2–60 keV) the best fit was obtained with a combination of Comptonization (Titarchuk 1994, ‘compTT’ in XSPEC) and blackbody components, along with a Gaussian representing fluorescent Fe K α emission centered around 6.5 keV. Other models typically used for pulsar spectra, including cutoff or broken power laws, or a power law with a blackbody component, generally gave worse fits. At high count rates, systematic errors in the PCA response are known to contribute to deviations from the model; for example, the reduced- χ^2 (χ^2_ν) for the Comptonization model fit to the highest flux spectrum was 3.41 (i.e. $\chi^2 = 511.7$ for 150 degrees of freedom). Adopting a systematic error of 1.7% (2% is often used for the PCA) was sufficient to reduce the fit statistic to 1.01. For comparison, a fit with this assumed systematic error and the same Gaussian component combined with a power law with a high-energy exponential cutoff gave $\chi^2_\nu = 1.52$, while a combination of blackbody and powerlaw components gave 5.29.

The PCA spectrum was significantly softer near the peak of the outburst compared to spectra obtained during the rise and decay (Fig. 2). This was primarily due to a decreased contribution from the $T_{\text{bb}} = 3\text{--}4$ keV blackbody component at higher fluxes, rather than a systematic variation in T_{bb} (for example). While T_{bb} is unusually high for a neutron star, examination of the unfolded spectra suggests that the requirement for the additional component may be due to intrinsic curvature of the approximately power law part of the Comptonized spectra. A similarly good fit was obtained with a very broad ($\sigma \approx 10$ keV) Gaussian component in place of the blackbody, and we note that the integrated flux is not sensitive to the nature of the additional component. Regardless of whether a blackbody or Gaussian component is used, the additional component is strongly required for the best fit.

The fitted column densities of neutral (unionized) matter measured over the outburst were consistent with the line-of-sight value estimated from HI/dust surveys, i.e., $\approx 10^{22}$ atoms cm $^{-2}$ (Dickey & Lockman 1990; Schlegel et al. 1998). Thus, to obtain flux estimates we fixed n_{H} at this value and integrated the best-fit spectral models comprising Comptonization and blackbody components over the 2–60 keV band. The results are shown in Fig. 1. At the peak of the outburst in 2001 February the 2–60 keV flux was $\sim 9 \times 10^{-9}$ ergs cm $^{-2}$ s $^{-1}$. The X-ray luminosity was therefore $\sim 1.1 \times 10^{38}$ ergs s $^{-1}$ for a source distance of 10 kpc.

4. PULSE TIMING ANALYSIS

4.1. Frequency measurements

To measure the long term frequency evolution of the pulsar we grouped together those *RXTE* observations

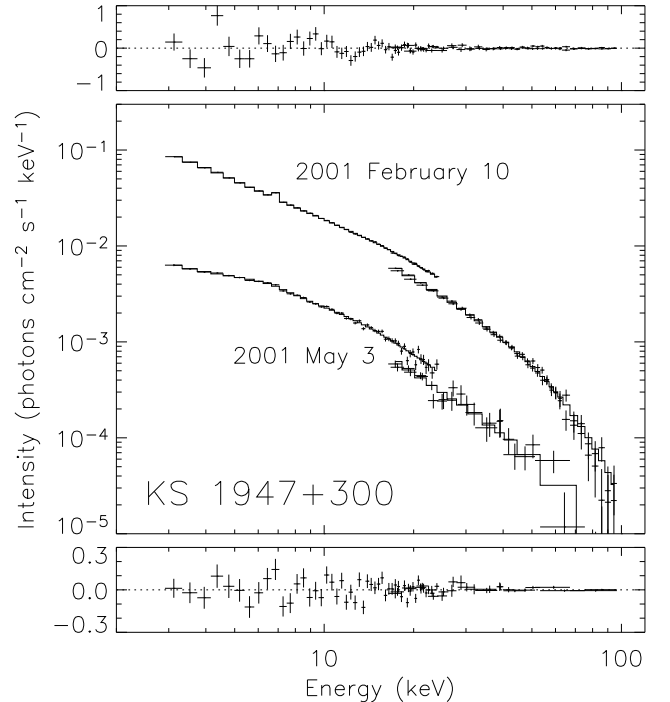


FIG. 2.— Representative photon spectra of KS 1947+300 from the peak (2001 February 10, or MJD 51950) and late in the decay (2001 May 3, MJD 52032) of the 2000–01 outburst. The effect of the instrumental responses have been removed (“unfolded”). Data from PCU #2 are shown, along with data from HEXTE clusters 1 and 2. For the 2001 May 3 observation, we rebinned the HEXTE spectra by a factor of 4. Error bars indicate the 1σ uncertainties. The top and bottom panels show the residuals to the model fit (units of normalized counts s $^{-1}$ keV $^{-1}$) for the 2001 February 10 and 2001 May 3 spectra, respectively.

that began within 8 hr of each other and would form a combined data set spanning less than 24 hr. The frequency was then estimated for each set of observations by fitting the 0.25-s time series with the function

$$F(t) = a_0 + a_1 \sin(\omega t) + a_2 \cos(\omega t) + a_3 \sin(2\omega t) + a_4 \cos(2\omega t) \quad (1)$$

over a grid of trial frequencies where the coefficients a_i were chosen to obtain the best fit for each frequency ω . The accuracy of each frequency measurement was estimated by the range of frequencies where $\chi^2 \leq \chi^2_{\text{min}} + 10$ (equivalent to $\approx 3\sigma$), where χ^2_{min} was the value of the goodness of fit statistic for the best fit.

We also used pulse frequencies determined from observations performed in 1994 with the BATSE instrument on the *Compton Gamma Ray Observatory*. The frequencies were obtained in the same way as those reported by Chakrabarty et al. (1995) except for being determined from 1-day rather than 2-day data sets. Data for the photon energy range 20–60 keV were used in this analysis.

The measured frequencies are shown in Fig. 3. In the ≈ 6 year interval between the 1994 and 2000 outbursts the neutron star rotational frequency decreased from 53.47 to 53.30 mHz, corresponding to a mean spin-down rate $\dot{f} \approx -8.2 \times 10^{-13}$ Hz s $^{-1}$. During the 2000–2001 outburst, there was a substantial overall increase in pulse frequency likely caused by accretion torques on the neutron star. An approximately sinusoidal periodic

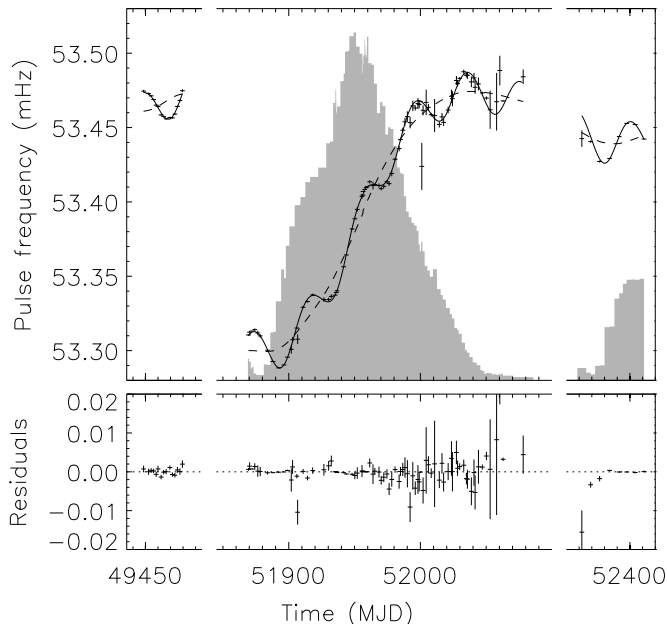


FIG. 3.— Barycenter-corrected pulse frequency for KS 1947+30 throughout the 1994 April outburst as measured by BATSE (Chakrabarty et al. 1995), and the 2000–01 and 2002 outbursts as seen by *RXTE*. The upper panel shows the frequency measurements and the best-fit model (solid line; see §4.1). The sum of model components representing the intrinsic neutron star spin frequency is shown as a dashed line. The lower panel shows the fit residuals. Error bars represent 1σ uncertainties. The grey histogram shows the PCA/HEXTE flux measurements.

variation is superposed on this increase; we naturally attribute it to Doppler shifts from orbital motion in a binary system.

4.2. Frequency Model

We fit the frequency measurements with a simple model comprising the effects of neutron star spin including the spin-up due to accretion torques and the apparent changes due to orbital Doppler shifts:

$$f(t) = f_{spin}(t) - \frac{2\pi f_{0j} a_x \sin i}{P_{orb}} (\cos l + g \sin 2l + h \cos 2l) \quad (2)$$

where $f_{spin}(t)$ is the time-dependent stellar spin frequency, f_{0j} is an initial spin frequency for each of the three observation epochs (BATSE, *RXTE* 2000–01, and *RXTE* 2002) denoted symbolically by j , $a_x \sin i$ is the projected orbital semimajor axis in units of light travel time, and P_{orb} is the orbital period. The coefficients $g (= e \sin \omega)$ and $h (= e \cos \omega)$ are to be interpreted as functions of the eccentricity e and the longitude of periastron ω . Finally, $l = 2\pi(t - T_{\pi/2})/P_{orb} + \pi/2$ is the mean longitude, with $T_{\pi/2}$ the epoch at which the mean longitude $l = \pi/2$. For a circular orbit, $T_{\pi/2}$ is the epoch of superior conjunction of the neutron star. The right-most term in parentheses of Eqn. 2 represents the orbital Doppler shifts to first order in e ; given the magnitudes of the uncertainties of our measurements, this should be an adequate approximation as long as $e \lesssim 0.2$.

The neutron star spin frequency may be affected by several physical mechanisms. Among these, accretion torques are likely to be most important. As a first approximation, we take the accretion torque to be pro-

portional to a power of the observed X-ray flux, i.e. $\tau_{acc} \propto F_X^\alpha$. This prescription is a limited generalization of models like those of Ghosh & Lamb (1979a,b) in which the torque is expected to be proportional to the accretion rate and, in turn, the flux raised to the power $6/7$.

To obtain a simple model of the X-ray flux F_X , we fitted a composite light curve consisting of daily averages of PCA/HEXTE 2–60 keV fluxes and ASM 1.5–12 keV intensities (renormalized to 2–60 keV fluxes) with the sum of a set of Gaussian components. The 2000–2001 outburst was modelled by the sum of 5 components, while the time interval of the 2002 observations was modelled by a single component. The parameter values defining the model are listed in Table 1. The individual components that describe the 2000–2001 outburst, as well as the total model, are plotted with the measured flux values in Fig. 1, lower panel. Over the 2000–2001 outburst, the root-mean-square difference between the measured fluxes and the model comprising five Gaussian components (nos. 2–6 of Table 1) was 0.32×10^{-9} ergs $\text{cm}^{-2} \text{s}^{-1}$. We also adopted an additional Gaussian component to represent the flux evolution during the 1994 BATSE observations. For that outburst, which lasted around 30 d, the source reached a maximum pulsed 20–60 keV flux of around 4.5×10^{-10} ergs $\text{cm}^{-2} \text{s}^{-1}$ on MJD 49465 (Chakrabarty et al. 1995). Broadband PCA/HEXTE spectra from the 2000–2001 outburst indicate that this likely corresponds to a 2–60 keV flux of around 1.9×10^{-9} ergs $\text{cm}^{-2} \text{s}^{-1}$ for a pulse fraction of 50% (see §4.3). Thus, we included a Gaussian component centered on MJD 49465 with a 1σ width of 10 d and peak flux of 1.9×10^{-9} ergs $\text{cm}^{-2} \text{s}^{-1}$.

We first tried to fit the measured frequencies with a simple model based on Eqn. 2 in which the time integral of τ_{acc} gives the change in intrinsic spin frequency. The best fit was poor ($\chi^2 = 2715$ for 101 degrees of freedom). There are a number of possible reasons for this, including (1) the spacing of the observations does not allow us to construct a flux model that reliably follows flux variations on short time scales ($\lesssim 10$ days), (2) the accretion rate may not be precisely proportional to the X-ray flux, and (3) the accretion torque in this simple model vanishes when $F_X = 0$. The latter property contradicts the observation of a net spin down during the ≈ 6 years between the BATSE and *RXTE* observations while the source was in quiescence, i.e. while $F_X \approx 0$. In order to allow the net model torque to be negative when $F_X = 0$, we have augmented the spin model with terms linear in time separately for each of the three epochs. The revised model of the intrinsic spin frequency is thus:

$$f_{spin}(t) = f_{0j} + b_j(t - t_{0j}) + \beta \int_{t_{0j}}^t F_X^\alpha(u) du + \Delta f_{gl}(t) \quad (3)$$

where f_{0j} and t_{0j} are the frequency and time, respectively, of the first frequency measurement for epoch j and $F_X(t)$ is the 2–60 keV flux in units of 10^{-9} ergs $\text{cm}^{-2} \text{s}^{-1}$. The adjustable parameters f_{0j} and b_j are set independently for each epoch while the power law index α and torque coefficient β , along with the orbital parameters, are adjustable parameters that apply globally to all three epochs. Further analysis (see §4.3) indicated that there was a rapid change in the intrinsic pulse

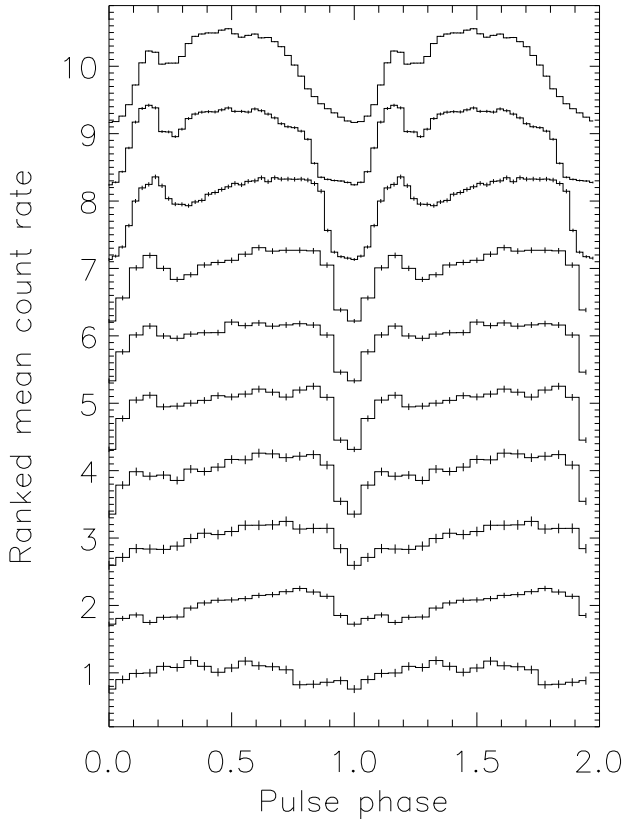


FIG. 4.— Representative pulse profiles from KS 1947+300 ranked by mean count rate. From top to bottom, the profiles are for the observations of 2001 Feb 10, Apr 5, May 6, May 12, May 17, May 18, May 21, May 27, 2000 Nov 28, and 2001 Jun 18 (MJD 51950, 52004, 52035, 52041, 52046, 52047, 52050, 52056, 51876 and 52078), respectively. The profiles have been rescaled by the mean rate and shifted in phase so that the minimum falls at phase 0.0. Each profile is plotted twice and shifted vertically for clarity.

frequency around $t_{\text{gl}} \simeq \text{MJD } 51956.41$. We therefore included the term $\Delta f_{\text{gl}}(t)$ which was assigned a value of zero for all measurements made prior to t_{gl} and a constant value of $1.83 \mu\text{Hz}$ for all measurements made afterwards. The magnitude of this frequency change was determined through a pulse arrival time analysis which is described below, and so was not a free parameter in the frequency model.

The model can be formulated so that it depends linearly on all the adjustable parameters except for α and P_{orb} . Thus, we searched a grid of points in α - P_{orb} space to determine the best-fitting parameter combination. When obtaining the best fit for each α - P_{orb} pair of values, all other parameters were allowed to vary in a linear χ^2 fitting process. The values of the parameters for the best-fit model are listed in Table 2. The model fits the data much better than our original simple model described above, although there are still significant residuals (Fig. 3). This is reflected in the reduced χ^2 value of 3.35. The fit results unambiguously yield the number of orbital cycles from the epoch of the BATSE observations to that of the *RXTE* observations, and thus an accurate orbital period of 40.415 d. We also note that the values of the coefficients b_j , i.e., the coefficients of the terms representing the values of \dot{f} at zero flux for each epoch, are negative as expected from the spin down inferred during

quiescence.

We first estimate the uncertainty in each fitted parameter of the frequency model from the range of values of that parameter that occur within the region defined by $\chi^2 = \chi_{\text{min}}^2 + \chi_{\nu}^2$ that we obtain when all parameters, except α , are allowed to vary. Here $\chi_{\nu}^2 = 3.35$ is the value of χ^2 per degree of freedom for the best fit. This χ^2 contour is that which yields 1σ errors when the uncertainties in the individual frequency measurements are scaled to give $\chi_{\nu}^2 = 1$, assuming correlations in the errors of different measurements are negligible. These estimates are given in column 4 of Table 2. These uncertainties do not reflect errors that could occur because (1) there could be correlations in the errors in the frequency measurements, (2) the flux model may not be precise, or (3) the model may not be formulated properly. We have attempted to crudely estimate the effects of the second possibility and the issue of possible systematic errors in general by varying the parameters describing the flux model one at a time while fixing all other flux model parameters at the values given in Table 1 and then redoing the fit for each new set of values. In this exercise we did not limit the range of values of the modified parameter to those values that give a good fit to the flux data. The magnitudes of the variation of each derived frequency model parameter in this exercise are given in column 5 of Table 2.

The fitted eccentricity of 0.033 indicates that the orbit is almost circular. Even so, a circular orbit fit ($e = 0$) results in a significantly poorer fit ($\chi_{\nu}^2 = 4.57$). The formal probability that the fit would yield $e \geq 0.033$ when the true orbit is perfectly circular is $\sim 1.1 \times 10^{-7}$; this is equivalent to a detection of non-zero e with 5σ confidence (cf. Lucy & Sweeney 1971). However, we note that the systematic uncertainty estimated in the exercise described above suggests that the significance of the measured eccentricity is closer to $\sim 2.5\sigma$.

4.3. Pulse Arrival Time Model

The pulse frequency fit takes advantage of the long baseline spanned by the observations, and yields an accurate determination of P_{orb} . However, that analysis did not take advantage of the relative phases of the pulsations from observation to observation. We therefore undertook a pulse arrival time analysis of the PCA data obtained in the first epoch of *RXTE* observations.

We first constructed a pulse profile for each observation by folding data in 0.25-s time bins using the pulse period predicted by a preliminary but reasonably accurate frequency model that included both intrinsic frequency changes and orbital Doppler shifts. Profiles for selected observations are shown in Fig. 4. The pulse shape evolved as the flux increased and decreased. At lowest flux the profile exhibited a single peak, with a narrow dip spanning 0.2 in phase forming the primary minimum. As the flux increased, a shallower secondary dip around 0.25 later in phase developed, so that the profile exhibited one narrow and one broad peak. The primary minimum also became progressively broader and asymmetric, with a more gradual ingress and egress. As the flux decreased following the peak, the same systematic variation in pulse profile was retraced in the opposite direction.

For the determination of pulse arrival times, we folded data from 512-s segments. We defined the pulse arrival

time as the epoch of maximum flux, which was determined by fitting a sinusoid to the pulse profile. The errors in the arrival times were estimated by varying the epoch of maximum flux in the fit over a grid to determine the interval in which $\Delta\chi^2 \leq 1$.

To make effective use of these arrival times, one must determine the number of pulsation cycles between each measured pulse arrival time. Thus, we used the preliminary frequency model noted above to estimate cycle counts. When observations were separated by longer than ~ 2 d it was not possible to unambiguously determine the cycle count using the frequency data alone. Instead, we performed a joint fit of both the frequency and arrival time data. For each long data gap, we fitted both frequencies and arrival times before and after the gap for times as far forward and backward as possible without introducing additional cycle-count ambiguities. Using this approach, we were able to determine the cycle counts from MJD 51914 to MJD 52062.

When the expression on the right in Eqn. 3 is substituted into Eqn. 2 and integrated, one obtains an expression for the pulse phase. Pulse arrival times may then be taken to be the times when the phase is an integer number of cycles. A constant of integration appears in going from frequency to phase; it may be taken as the arrival time of a given pulse.

We then fit the arrival times within the range over which we can unambiguously phase-connect the observations, as well as the frequency data before and after. The best-fit model did not fit the data well, as indicated by the large value of reduced χ^2 . One major reason for the lack of agreement between the model and the measured arrival times was an instance, around MJD 51956.4, where the pulse frequency changed rather rapidly (see Fig. 5). The event is apparent in both the frequency measurements and in the arrival time (or, equivalently, pulse phase) residuals from a fit calculated using only pulse arrival times prior to the event. Examination of pulse profiles revealed no significant pulse shape change around the time of the event.

The residuals were consistent with a stepwise change of frequency of $\Delta f \approx +1.8 \mu\text{Hz}$ occurring around MJD 51956.41 (such a change is included in the frequency fit; see §4.2). In order to obtain limits on the magnitude and duration of this event, we fit a model to the arrival time data that included a step in frequency Δf_{gl} that occurred via a constant frequency derivative over a time interval Δt_{gl} centered at time t_{gl} . These parameters, as well as low-order polynomial terms in time, were allowed to vary in the fitting process while the orbital parameters and the torque coefficient were fixed at the values determined from the best-fit frequency model. When this fit was performed on the arrival time data from the 7.8 day time interval MJD 51952.03 through 51959.83, we obtain $\Delta f_{\text{gl}} = 2.01 \pm 0.04 \mu\text{Hz}$, $t_{\text{gl}} = \text{MJD } 51956.393 \pm 0.01$, and $\Delta t_{\text{gl}} < 0.4$ days, where the errors have been scaled by the square root of $\chi^2_{\nu} = 0.69$. When this fit was performed on the arrival time data from a shorter time interval, i.e., MJD 51955.6 through MJD 51959.1, the best fit is obtained for $\Delta f_{\text{gl}} = 1.83 \pm 0.09 \mu\text{Hz}$, $t_{\text{gl}} = \text{MJD } 51956.416 \pm 0.014$, and $\Delta t_{\text{gl}} < 0.5$ days, again where the errors have been scaled by the square root of $\chi^2_{\nu} = 0.67$. The best-fit values of the parameters which describe the glitch

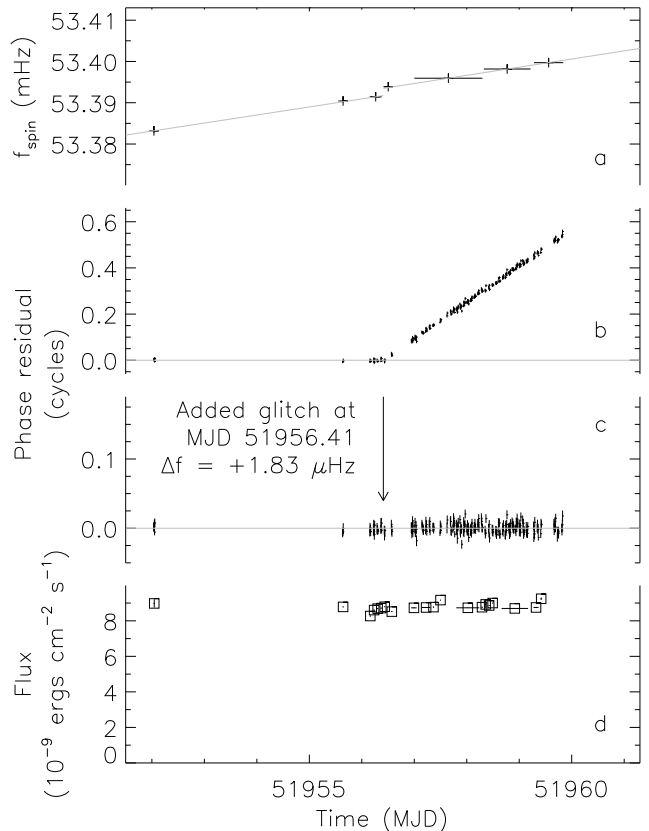


FIG. 5.— Pulse frequencies, phase residuals, and X-ray intensities around the time of the glitch. (a) Measured pulse frequency corrected for the binary orbit with error bars corresponding to 3σ confidence intervals. (b) Phase residuals calculated from a best-fit model that does not include a component representing the glitch. (c) Phase residuals from a full model that does include a component representing the glitch. Note the difference in scale between panels b and c. (d) The 2–60 keV band source flux.

do not appear to depend, within limits, on the length of the data set. The full sets of model parameters of both fits may be found in Table 3. We note that the parameters listed in Table 3 are consistent with an instantaneous change in frequency.

5. DISCUSSION

We measured the flux and pulse frequency evolution of the X-ray pulsar KS 1947+300 through a large outburst in 2000–01, as well as in a smaller outburst in 2002. We fitted the measured pulse frequencies and arrival times to derive orbital parameters, and to determine the temporal variation of the intrinsic spin frequency of the neutron star. We found that the pulsar revolves in a nearly circular orbit ($e = 0.033 \pm 0.013$) with orbital period 40.415 ± 0.010 d, and projected semi-major axis 137 ± 3 lt-sec. This orbital period is significantly shorter than that derived from analysis of the pre-outburst ASM light curve, 41.7 ± 0.1 days (Levine & Corbet 2000). Although it is clear that the value based on pulse timing is correct, the basis of the discrepancy is not clear. We note that the X-ray light curves of other Be-star/neutron star binaries sometimes do contain quasiperiodic variations that are asynchronous with the orbits (e.g., GS 0834–430, Wilson et al. 1997; XTE J1946+274, Wilson et al. 2003).

If we assume that the neutron star mass $M_X = 1.4M_{\odot}$,

then the X-ray mass function of $f_X = 1.71 \pm 0.04 M_\odot$ implies a companion mass of at least $3.4 M_\odot$ (for an inclination $i \leq 90^\circ$). We do not find eclipses in either the ASM or the PCA light curves, and can confidently conclude that the system is not eclipsing, thus ruling out inclinations $\gtrsim 85^\circ$. Companion masses $M_c = 5, 10, \text{ or } 20 M_\odot$, imply inclinations of $57^\circ, 38^\circ, \text{ or } 28^\circ$ respectively. This range of masses and inclinations is compatible with the B0Ve spectral type of the optical counterpart (Negueruela et al. 2003).

The wide orbital separation and low eccentricity place KS 1947+300 within the small class of neutron stars with high-mass binary companions which almost certainly did not receive large “kicks” during the supernovae which led to their formation (Pfahl et al. 2002). The optical counterpart appears to be a Be star that is not highly evolved. Thus its radius is most likely much smaller than the radius of its Roche lobe, i.e., than 104, 141, or 191 lt-s for $M_X = 1.4 M_\odot$ and $M_c = 5, 10, \text{ or } 20 M_\odot$, respectively. Furthermore, the wide separation and relatively small size of the companion suggest that it is unlikely that tidal effects have circularized the orbit since the supernova event wherein the neutron star was formed. If the pre-supernova orbit was circular, the measured eccentricity $e \sim 0.03$ suggests that the mass ejected in the supernova must have been rather small, i.e., $\Delta M/M_{\text{final}} < 0.03$, where M_{final} , the post-supernova system mass, could be as large as $20M_\odot$. The low eccentricity of this system clearly presents a number of difficulties.

An outburst of KS 1947+300 was seen with BATSE in 1994, and no other outburst was reported until that of 2000–2001. BATSE operated continuously until 2000 May, while the *RXTE* ASM has operated more or less continuously since early 1996. BATSE would most likely have detected any pulsed flux greater than ≈ 20 mCrab in the 30–75 keV band (equivalent to a flux 2×10^{-10} ergs $\text{cm}^{-2} \text{s}^{-1}$) that was present for more than a few days. The ASM would most likely have detected any outburst longer than ≈ 5 d that reached a strength of ≈ 1 ASM count s^{-1} (equivalent to 13 mCrab or to a 2–12 keV band flux 3×10^{-10} ergs $\text{cm}^{-2} \text{s}^{-1}$). Thus, as was also discussed by Negueruela et al. (2003), we can rule out the occurrence of a moderate to strong outburst in the intervening time, although it is possible that weak outbursts could have been missed.

From the end of the outburst in 1994 to the beginning of the outburst in late 2000, the pulsar frequency decreased from 53.47 to 53.30 mHz. The average frequency derivative during this interval was $\dot{f} = -0.8 \times 10^{-12}$ Hz s^{-1} . Spin-down in quiescence likely arises from the dominance of magnetic torques contributed by field lines which thread the accretion disk outside the corotation radius (e.g. Ghosh & Lamb 1979a,b). Alternatively, negative torques may arise from the “propeller effect” (Illarionov & Sunyaev 1975). We note that the magnitude of the quiescent spin-down was comparable to that measured for at least one other pulsar, A 0535+26, of $-(2.2 \pm 0.6) \times 10^{-13}$ Hz s^{-1} (Finger et al. 1994). While the values of b_j for each epoch (see Table 2) are comparable to, or significantly larger than the quiescent spin-down, we caution that it is not correct to interpret these parameters independently from the torque model. The b_j are coefficients of terms we used to augment the accretion

torque integral in equation 3, so as to more accurately model the intrinsic spin changes of the neutron star. The integral alone would give zero torque only at zero flux, whereas the various negative fitted values of the b_j indicate that zero torque corresponds to non-zero flux at a different level for each epoch.

The 2–60 keV flux of KS 1947+300 peaked at 9×10^{-9} ergs $\text{cm}^{-2} \text{s}^{-1}$ in 2001 February. This flux implies an X-ray luminosity of 1.1×10^{38} ergs s^{-1} for a source distance of 10 kpc. Given this accretion luminosity, a neutron star of mass $M_X = 1.4 M_\odot$, radius $R = 10$ km, magnetic moment $\mu = 1 \times 10^{30}$ G cm^3 (equivalent to an equatorial surface magnetic field strength of 10^{12} G), and moment of inertia $I = 1 \times 10^{45}$ g cm^2 , a standard theoretical treatment (Eqn. 15 of Ghosh & Lamb 1979b; Joss & Rappaport 1976) predicts $\dot{f} = 1.5 \times 10^{-11}$ Hz s^{-1} whereas the intrinsic frequency derivative around the time of maximum flux obtained from our pulse timing results is $\dot{f} \simeq 2.3 \times 10^{-11}$ Hz s^{-1} . These values are consistent given the simple nature of the theoretical estimate, the possibility of deviations from the assumed neutron star parameters, and the uncertainty in the distance to the system.

We found evidence for a particularly rapid variation of the pulse frequency around MJD 51956.41. The phase residuals around this episode were minimized by including a change in frequency of $\Delta f \approx +1.8$ μHz that occurred at a uniform rate over a time interval $\Delta t \lesssim 10$ hr. The frequency change corresponds to a fractional change $\Delta f/f \approx 3.7 \times 10^{-5}$. If the frequency change occurred at a constant rate over a 10 hr interval, then the intrinsic neutron star pulse frequency derivative must have reached at least 4.8×10^{-11} Hz s^{-1} , more than twice as large as the maximum inferred from the torque model, 2.3×10^{-11} Hz s^{-1} . We note that this event occurred close to the time of peak flux and, therefore, when the accretion torque was near its maximum value. While it is possible that the abrupt increase in frequency arose from a brief episode of enhanced accretion, we found no evidence for the increase in flux which might be expected as an immediate consequence (see Fig. 5). A transient flux increase could have been missed during the ≈ 4 hr gap (MJD 51956.39 to 51956.56) between the observations closest to the estimated time of the glitch. However, the increase in X-ray luminosity required to explain the magnitude of the glitch would be a factor of ≈ 2 , sufficient to exceed the Eddington limit for a canonical neutron star at 10 kpc distance. Furthermore, four ASM dwells at MJD 51956.51 indicate a flux of 7.3 ± 0.6 counts s^{-1} , consistent with the level before and after the gap.

This event may have arisen from a sudden change in the spin frequency of the neutron star, analogous to the “glitches” observed in other types of neutron stars. However, there are also some significant differences between the glitch in KS 1947+300 and those in radio pulsars and AXPs. First, in contrast to radio pulsar glitches, which frequently exhibit a change in the spin-down rate \dot{f} following a glitch, we measured consistent values of \dot{f} before and after MJD 51956.41. Second, the fractional change in frequency of 3.7×10^{-5} in the KS 1947+300 glitch is around an order of magnitude larger than the typical value for “giant” glitches in radio pulsars (Krawczyk et al. 2003). Finally, what is more

puzzling is that the frequency change in KS 1947+300 was in the same sense as the mean spin-up around that time, i.e. the glitch resulted in a brief *acceleration* of the spin-up rate by at least a factor of 2 to 3. Since the neutron star was spinning up at the time of the glitch, one might expect that the core would be rotating more slowly than the crust, so that a glitch would cause a sudden decrease in the pulse frequency. However, a long history of spin up and spin down episodes may have left the core spinning faster than the crust at the time of the glitch. The BATSE observations indeed show that the pulse frequency in 1994 was higher than the pulse frequency at the time of the glitch.

This is the first reported glitch in an accretion-powered pulsar. If such events occur in other accreting neutron stars, why have they not been detected previously? The main reason may be that such events are simply difficult to detect; indeed, there are a number of conditions which are required for the detection of glitches in either accreting or rotation-powered neutron stars. The pulsars must be monitored over a period of days, with observations being done at least several times per day. This is often more difficult to accomplish from space-based X-ray satellites than from ground-based radio observatories. Also, the extraction of pulse frequencies from previous X-ray observations of pulsars have sometimes been done using 1 day or longer integration time intervals, which makes it difficult to detect μHz frequency changes occurring on time scales of hours or less. Sudden frequency changes could be lost among the other frequency changes from torque variations which typically take place on longer time scales.

We can estimate the sensitivity for the detection of a sudden frequency change from a set of observations. For this purpose we assume that two estimates of the pulse frequency are made, one before and one after the time of a possible sudden change. For simplicity, we further assume that each frequency estimate is made from a set of N equally-spaced observations made over an interval of length T , that each observation yields a phase estimate with 1σ uncertainty σ_ϕ , and that there are no pulse counting ambiguities left unresolved. In this case the 1σ uncertainty in the difference of the two frequency estimates is given by

$$\sigma_f \sim a \left(\frac{\sigma_\phi}{0.1 \text{ cycle}} \right) \left(\frac{T}{1 \text{ d}} \right)^{-1} N^{-1/2} \mu\text{Hz} \quad (4)$$

where a is a factor of order unity. The length of the time interval T over which the frequency estimates are to be made is limited by the frequency changes generally ascribed to accretion torque variability. Equation 4 indicates that the detection of a $\sim 1 \mu\text{Hz}$ glitch requires, for example, $N \sim 10$ observations over the course of a few days with each observation yielding a modest accuracy phase measurement.

The BATSE instrument on the Compton Gamma-Ray Observatory monitored many accretion-powered pulsars over the course of 9 years with a sensitivity of $\sim 1 \mu\text{Hz}$ per day in favorable cases (Bildsten et al. 1997). Frequencies were reported for every day or every few days that pulsations were detected (Chakrabarty et al. 1997a, Finger et al. 1999, Koh et al. 1997, Chakrabarty et al. 1997b). Though the BATSE results have not led to the report of any glitch, it is possible that some of the monitored pulsars did exhibit glitches that were not easily noticed because of the large frequency variations on time scales of days and weeks.

A second possibility is that such events may also be quite rare. In this regard, we note that KS 1947+300 was accreting near the Eddington limit when this glitch occurred. If glitches in accretion-powered pulsars only occur under such circumstances, then the opportunities for their detection would be quite limited, since the times when Galactic pulsars are observed to be accreting near the Eddington limit are relatively infrequent. Clearly, new analyses of archival data and additional observations are called for in order to find other examples of glitches and to determine how often such events occur in accreting neutron stars.

This research has made use of data obtained through the High Energy Astrophysics Science Archive Research Center Online Service, provided by the NASA/Goddard Space Flight Center. We thank D. Chakrabarty for providing pulse frequencies from the 1994 BATSE observations and for helpful comments on the manuscript, and S. Rappaport for helpful comments. This work was supported in part by NASA Contract NAS5-30612 and by the NASA Long Term Space Astrophysics program under grant NAG 5-9184.

REFERENCES

- Anderson, P. W. & Itoh, N. 1975, *Nature*, 256, 25
 Borozdin, K., Gilfanov, M., Sunyaev, R., Churazov, E., Loznikov, V., Yamburenko, N., Skinner, G. K., Patterson, T. G., Willmore, A. P., Emam, O., Brinkman, A. C., Heise, J., In'tzand, J. J. M., & Jager, R. 1990, *PAZh*, 16, 804
 Chakrabarty, D., Koh, T., Bildsten, L., Prince, T. A., Finger, M. H., Wilson, R. B., Pendleton, G. N., & Rubin, B. C. 1995, *ApJ*, 446, 826
 Dickey, J. M. & Lockman, F. J. 1990, *ARA&A*, 28, 215
 Finger, M. H., Cominsky, L. R., Wilson, R. B., Harmon, B. A., & Fishman, G. J. 1994, in *AIP Conf. Proc.* 308: The Evolution of X-ray Binaries, 459
 Ghosh, P. & Lamb, F. K. 1979a, *ApJ*, 232, 259
 —. 1979b, *ApJ*, 234, 296
 Gruber, D. E., Blanco, P. R., Heindl, W. A., Pelling, M. R., Rothschild, R. E., & Hink, P. L. 1996, *A&AS*, 120, C641
 Illarionov, A. F. & Sunyaev, R. A. 1975, *A&A*, 39, 185
 Jahoda, K., Swank, J. H., Giles, A. B., Stark, M. J., Strohmayer, T., Zhang, W., & Morgan, E. H. 1996, *Proc. SPIE*, 2808, 59
 Joss, P. C. & Rappaport, S. A. 1976, *Nature*, 264, 219
 Kaspi, V. M. & Gavriil, F. P. 2003, *ApJ*, 596, L71
 Kaspi, V. M., Gavriil, F. P., Woods, P. M., Jensen, J. B., Roberts, M. S. E., & Chakrabarty, D. 2003, *ApJ*, 588, L93
 Krawczyk, A., Lyne, A. G., Gil, J. A., & Joshi, B. C. 2003, *MNRAS*, 340, 1087
 Levine, A. & Corbet, R. 2000, *IAU Circ.*, 7523
 Levine, A. M., Bradt, H., Cui, W., Jernigan, J. G., Morgan, E. H., Remillard, R., Shirey, R. E., & Smith, D. A. 1996, *ApJ*, 469, L33
 Negueruela, I., Israel, G. L., Marco, A., Norton, A. J., & Speziali, R. 2003, *A&A*, 397, 739
 Pfahl, E., Rappaport, S., Podsiadlowski, P., & Spruit, H. 2002, *ApJ*, 574, 364
 Ruderman, M. 1976, *ApJ*, 203, 213
 Schlegel, D. J., Finkbeiner, D. P., & Davis, M. 1998, *ApJ*, 500, 525
 Skinner, G. K. 1989, *IAU Circ.*, 4850
 Swank, J. & Morgan, E. 2000, *IAU Circ.*, 7531
 Titarchuk, L. 1994, *ApJ*, 434, 570

TABLE 1
GAUSSIAN COMPONENTS OF THE X-RAY LIGHT CURVE

Data set	Component number	Center (MJD)	Width ^a (d)	Peak Intensity (10^{-9} ergs cm^{-2} s^{-1})
BATSE	1	49465.0	10.0	1.92
<i>RXTE</i>	2	51855.0	10.0	1.92
	3	51904.2	10.0	2.72
	4	51945.4	23.6	6.43
	5	51974.9	32.1	4.12
	6	52020.5	7.4	0.449
	7	52405.0	17.0	2.88

^aStandard deviation

TABLE 2
FREQUENCY MODEL PARAMETERS FOR KS 1947+30

Parameter	Epoch	Fit Value	Uncertainty ^a	Uncertainty due to Flux Model ^b
t_{01} (MJD)	BATSE	49448.5
f_{01} (mHz)	BATSE	53.4610	0.0015	0.0010
b_1 (10^{-12} Hz s^{-1})	BATSE	-1.9	0.9	6.2
t_{02} (MJD)	<i>RXTE</i> 1	51869.397
f_{02} (mHz)	<i>RXTE</i> 1	53.3000	0.0003	0.0005
b_2 (10^{-12} Hz s^{-1})	<i>RXTE</i> 1	-3.4	0.2	0.6
t_{03} (MJD)	<i>RXTE</i> 2	52362.115
f_{03} (mHz)	<i>RXTE</i> 2	53.4448	0.0008	0.0036
b_3 (10^{-12} Hz s^{-1})	<i>RXTE</i> 2	-7.2	0.3	3.5
t_{gl} (MJD)	All	51956.416
Δf_{gl} (Hz)	All	1.83×10^{-6}
α	All	0.75	0.02	...
β^c	All	4.35×10^{-7}	0.07×10^{-7}	0.21×10^{-7}
P_{orb} (d)	All	40.415	0.007	0.010
$a_{\infty} \sin i$ (lt-s)	All	137.4	1.2	3.0
$T_{\pi/2}$ (MJD)	All	51985.31	0.07	0.06
e	All	0.034	0.007	0.013
ω ($^{\circ}$)	All	33	3	...
$f_X(M)$ (M_{\odot})	All	1.71	0.04	...
$\chi^2/N(\text{DoF})$			329/98	

^aThe range of variation of the parameter values that occur within the $\chi^2 = \chi_{\text{min}}^2 + \chi_{\text{min}}^2/N(\text{DoF})$ region that applies when all other frequency model parameters, except for α , are allowed to vary.

^bThe range of variation of the parameter for the best fit when the parameters describing the flux model (Table 1) are varied one at a time (see text).

^cTorque coefficient in units of Hz day^{-1}

TABLE 3
PULSE ARRIVAL TIME MODELS AROUND THE GLITCH^a

Parameter	Value ^b – Fit 1	Value ^b – Fit 2
Time interval (MJD)	51952.03–51959.83	51955.6–51959.1
t_0 (MJD)	51869.397	51869.397
f_0 (mHz)	53.29791 ± 0.00027	53.2976 ± 0.0014
b (10^{-12} Hz s ⁻¹)	-15.6 ± 0.2	-15.4 ± 1.0
t_{gl} (MJD)	51956.393 ± 0.010	51956.416 ± 0.014
Δt_{gl} (days)	< 0.4	< 0.5
Δf_{gl} (μ Hz)	2.01 ± 0.04	1.83 ± 0.09
$\chi^2/N(\text{DoF})$	154.0/224	121.7/183

^aThe following parameters were held fixed at the indicated values determined from the frequency model fitting: $P_{\text{orb}} = 40.415$ d; $a_x \sin i = 137.3$ (lt-s); $T_{\pi/2} = (MJD) 51985.31$; $g = 0.018928$; $h = 0.027032$; $\alpha = 0.75$; $\beta = 4.35 \times 10^{-7}$ Hz day⁻¹. The values of g and h correspond to an eccentricity $e = \sqrt{(g^2 + h^2)} = 0.033$. The uninteresting parameter ϕ_0 is not listed here.

^bParameters without uncertainties were held fixed at the given values. The indicated uncertainties correspond to 1σ confidence levels obtained from evaluation of $\Delta\chi^2 = \chi^2_{\nu}$. Upper limits correspond to 2σ confidence limits.